MOLECULAR AND CELLULAR BIOLOGY, Mar. 2011, p. 1134–1144 Vol. 31, No. 6
0270-7306/11/$12.00 doi:10.1128/MCB.01025-10

Cardiac Tissue-Restricted Deletion of Plakoglobin Results in Progressive Cardiomyopathy and Activation of β-Catenin Signaling▽†

Jifen Li,[1] David Swope,[1] Natalia Raess,[2] Lan Cheng,[1] Eliane J. Muller,[2] and Glenn L. Radice[1]*

Center for Translational Medicine, Department of Medicine, Thomas Jefferson University, Philadelphia, Pennsylvania,[1] and Molecular Dermatology, Institute of Animal Pathology, Vetsuisse Faculty, University of Bern, Bern, Switzerland[2]

Received 1 September 2010/Returned for modification 19 September 2010/Accepted 3 January 2011

Mutations in the *plakoglobin* (*JUP*) gene have been identified in arrhythmogenic right ventricular cardiomyopathy (ARVC) patients. However, the mechanisms underlying plakoglobin dysfunction involved in the pathogenesis of ARVC remain poorly understood. Plakoglobin is a component of both desmosomes and adherens junctions located at the intercalated disc (ICD) of cardiomyocytes, where it functions to link cadherins to the cytoskeleton. In addition, plakoglobin functions as a signaling protein via its ability to modulate the Wnt/β-catenin signaling pathway. To investigate the role of plakoglobin in ARVC, we generated an inducible cardiorestricted knockout (CKO) of the *plakoglobin* gene in mice. Plakoglobin CKO mice exhibited progressive loss of cardiac myocytes, extensive inflammatory infiltration, fibrous tissue replacement, and cardiac dysfunction similar to those of ARVC patients. Desmosomal proteins from the ICD were decreased, consistent with altered desmosome ultrastructure in plakoglobin CKO hearts. Despite gap junction remodeling, plakoglobin CKO hearts were refractory to induced arrhythmias. Ablation of plakoglobin caused increase β-catenin stabilization associated with activated AKT and inhibition of glycogen synthase kinase 3β. Finally, β-catenin/TCF transcriptional activity may contribute to the cardiac hypertrophy response in plakoglobin CKO mice. This novel model of ARVC demonstrates for the first time how plakoglobin affects β-catenin activity in the heart and its implications for disease pathogenesis.

Arrhythmogenic right ventricular cardiomyopathy (ARVC [Mendelian Inheritance in Man database code MIM107970]) is a hereditary heart muscle disease that causes sudden cardiac death in young people and athletes (4, 42). The pathological hallmark of ARVC consists of progressive loss of cardiomyocytes, myocardial degeneration, and compensatory replacement with fibrofatty tissue. These changes are often associated with inflammatory infiltrates, which may be involved in triggering life-threatening arrhythmias. The end-to-end connection between cardiomyocytes is maintained by the intercalated disc (ICD) structure. So far, 40% of patients with ARVC have been identified with a mutation in one of the five major components of the cardiac desmosome, an intercellular junction residing within the ICD (9, 41). However, the mechanisms underlying desmosomal protein dysfunction involved in the pathogenesis of ARVC remain poorly understood.

Desmosomes and adherens junctions are intercellular adhesive junctions that anchor intermediate filaments and the actin cytoskeleton, respectively, at the ICD. The adhesive junctions provide mechanical attachment between the cells, thus maintaining the structural and functional integrity of the heart. Cardiac desmosomes consist of desmosomal cadherins, armadillo proteins, and plakins (16). Desmosomal cadherins, desmoglein-2 (DSG-2), and desmocollin-2 (DSC-2) form extracellular connections by homophilic and heterophilic binding with cadherins on a neighboring cell. The cytoplasmic tails of desmosomal cadherins bind to the armadillo proteins plakoglobin (PG) and plakophilin-2 (PKP-2), which in turn bind to the plakin protein desmoplakin (DP). DP links desmosomes to intermediate-filament desmin. In the classic adherens junction model, the cytoplasmic tail of N-cadherin interacts in a mutually exclusive manner with either β-catenin or PG. β-Catenin or PG links cadherins to α-catenin, and α-catenin interacts with either the cadherin/catenin complex or the actin cytoskeleton (12). The gap junction is another intercellular junction responsible for cell-cell communication and electrical coupling by mediating small-molecule and ion transfer between cardiomyocytes. Connexin 43 (Cx43) is the most abundant connexin isotype localized in gap junctions of the heart (41). The different junctional complexes must be properly organized in the ICD to preserve normal mechanical and electrical function of the heart.

PG was the first component of the desmosome to be implicated in the pathogenesis of ARVC (37). Studies of individuals from the Greek island of Naxos (Naxos disease) identified an autosomal recessive form of ARVC with palmoplantar keratoderma and woolly hair. Gene sequencing revealed a homozygous 2-bp deletion (2157-2158delGT) in the *plakoglobin* (*JUP*) gene in affected individuals (31). A study of a German family recently reported the first dominantly inherited *PG* gene mutation (S39_K40insS) to cause ARVC without cutaneous abnormalities (2). Both mutant forms of PG fail to localize properly at the ICD, and the junctional components DP and Cx43 are significantly reduced at the ICD in these patients. Ultrastructural investigation showed ICD remodeling with mislocalization and a decreased number of desmosomes (2, 5). Importantly, a reduced immunoreactive PG signal at the ICD is a

* Corresponding author. Mailing address: Center for Translational Medicine, Department of Medicine, Rm. 309, College Bldg., 1025 Walnut St., Philadelphia, PA 19107. Phone: (215) 503-5157. Fax: (215) 503-5731. E-mail: glenn.radice@jefferson.edu.

† Supplemental material for this article may be found at http://mcb.asm.org/.

▽ Published ahead of print on 18 January 2011.

consistent feature in patients with dominant mutations in a variety of desmosomal genes, making PG an important diagnostic tool for ARVC in affected individuals (3).

PG and the homologous protein β-catenin share 88% amino acid identity and bind to common protein partners; therefore, they functionally compete with each other (51). The majority of PG and β-catenin is engaged at adherens junctions and/or desmosomes, linking adhesion receptors to the cytoskeleton. The cytoplasmic pool, or nonjunctional, catenins are targeted by glycogen synthase kinase 3α/β (GSK-3α/β) N-terminal phosphorylation for degradation by the ubiquitin-proteasome system. Stabilization of cytoplasmic β-catenin following Wnt ligand stimulation leads to its nuclear accumulation, binding with T cell factor/lymphoid enhancer factor (TCF/LEF) transcription factors, and transactivation of β-catenin/TCF/LEF target genes. In the adult heart, β-catenin/TCF/LEF-dependent gene expression has been shown to regulate both physiologic and pathological growth (i.e., hypertrophy) (7). In terminally differentiated cardiomyocytes, β-catenin is stabilized by a Wnt-independent mechanism involved in the recruitment of activated protein kinase B (PKB/AKT) to the β-catenin degradation complex (18). In addition, PG can also bind to TCF/LEF and either activate or suppress gene transcription, depending on the targets and cellular context (28, 33, 50, 51). For example, PG was shown to suppress the expression of c-Myc in epidermal keratinocytes in a Lef-1-dependent manner (47).

In the present study, we analyzed a conditional mouse model with cardiorestricted deletion of the *PG* gene to investigate the role of PG in the pathogenesis of ARVC. We demonstrate for the first time that disruption of junctional integrity leads to myocyte loss, inflammation, activation of β-catenin signaling, and pathological hypertrophy, thus representing a novel model of ARVC.

MATERIALS AND METHODS

Generation of PG conditional-knockout (CKO) mice. To generate a targeting vector, a bacterial artificial chromosome library derived from a 129Sv mouse strain was screened with a PG probe. A *loxP* site was inserted upstream of exon 1, and a *loxP* site and an FRT-flanked neomycin cassette were introduced into intron 1 of the PG gene. The vector was linearized with NotI and electroporated into TL-1 129Sv embryonic stem (ES) cells, and 150 G418-resistant clones were examined by Southern blot analysis. Three ES cell clones had undergone homologous recombination at the *PG* locus. PCR analysis demonstrated that all three targeted ES cell clones contained the distal *loxP* site. The targeted ES cells were injected into C57BL/6J blastocysts to generate chimeric mice. The PG CKO mice were analyzed in a mixed 129Sv-C57BL/6J genetic background. The floxed mice were genotyped by PCR. The following primer pair was used to distinguish the wild-type (WT) and floxed alleles: PGloxpF, 5′-AAG AAA TAC CCA CGG CTC CT-3′; PGloxpR, 5′-GCT CCA GGG AGA AAC AGA CA-3′. The WT and floxed PCR products correspond to 190 and 224 bp, respectively. The following primer pair was used to detect the deleted allele: PGloxpF, 5′-AAG AAA TAC CCA CGG CTC CT-3′; PGdeltaR, 5′-TTC GAC GGA GTA GCA TAG GG-3′. The PCR product was 250 bp. The FRT-flanked neomycin cassette was removed from the *PG* floxed allele by breeding to transgenic mice expressing the enhanced version of the site-specific recombinase FLP (39). To induce Cre-mediated recombination, adult alpha-myosin heavy chain (α-MHC)/MerCreMer $PG^{flox/flox}$ mice were treated with tamoxifen (Tam; Sigma) by intraperitoneal injection once a day for 5 consecutive days at a dosage of 2 mg/25 g mouse per day. Tam (20 mg/ml) was dissolved in corn oil (Sigma) by heating to 37°C for 1 h. All animal procedures and experiments were performed in accordance with the guidelines of the IACUC of Thomas Jefferson University.

Histological analysis. Hearts were isolated and fixed in 4% paraformaldehyde, dehydrated, and embedded in paraffin. Global heart architecture was determined from longitudinal 6-μm deparaffinized sections stained with hematoxylin and eosin (H&E). Fibrosis was detected with Masson's trichrome stain. Cross-sectional cell area measurements were obtained at the level of the nucleus in cross-sectioned, H&E-stained myocytes. Surface areas were quantified using NIS-Elements D software (Nikon). A minimum of 100 myocytes from three to five different animals were quantified for each experimental group.

RNA isolation, reverse transcription, and quantitative real-time PCR. Total RNA was isolated from whole heart tissue using TRIZOL reagent according to the manufacturer's protocol (Invitrogen). cDNA was synthesized using the iScript cDNA synthesis kit (Bio-Rad), and PCR was performed with iQ SYBR Green Supermix (Bio-Rad) in the MyiQ single-color real-time PCR detection system (Bio-Rad). Gene expression was represented by the ΔC_T value normalized to the reference gene for glyceraldehyde 3-phosphate dehydrogenase (GAPDH). The $\Delta\Delta C_T$ value of each target gene was then calculated by subtraction of the average ΔC_T from the control group. Finally, the *n*-fold difference was calculated by using the formula $2^{-\Delta\Delta CT}$. Data from 3 to 12 heart samples were collected and analyzed in triplicate. The primers used for real-time PCR were for atrial natriuretic protein (ANP; forward, 5′-CATCACCCTGGGCTTCTTCCT-3′; reverse, 5′-TGGGCTCCAATCCTGTCAATC-3′), brain natriuretic protein (BNP; forward, 5′-GCGGCATGGATCTCCTGAAGG-3′; reverse, 5′-CCCAG GCAGAGTCAGAAACTG-3′), β-MHC (forward, 5′-ATGTGCCGGACCTTG GAA-3′; reverse, 5′-CCTCGGGTTAGCTGAGAGATCA-3′), α-MHC (forward, 5′-GGCACAGAAACACCTGAAGA-3′; reverse, 5′-CATTGGCATGGA CAGCATCATC-3′), cyclin D1 (forward, 5′-CCACAGATGTGAAGTTCATTT CCA-3′; reverse, 5′-GCAGTCCGGGTCACACTTG-3′), c-Myc (forward, 5′-G CCCCTAGTGCTGCATGAG-3′; reverse, 5′-CCACAGACACCACATCAATT TCTT-3′), c-Fos (forward, 5′-CCGACTCCTTCTCCAGCAT-3′; reverse, 5′-TC ACCGTGGGGATAAAGTTG-3′), TCF-4 (forward, 5′-AACGGAACAGACA GTATAATGG-3′; reverse, 5′-CACAGGAGTTGAAGGATTGG-3′), axin-2 (forward, 5′-GAGTAGCGCCGTGTTAGTGACT-3′; reverse, 5′-CCAGGAAA GTCCGGAAGAGGTATG-3′), Cx43 (forward, 5′-TGGCCTGCTGAGAACC TACA-3′; reverse, 5′-CACTCAGGCTGAACCCATAGATG-3′), plakoglobin (forward, 5′-CCTGTGGACTCTGCGCAAT-3′; reverse, 5′-GACCAGGATCT TCAGCACACTCT-3′), β-catenin (forward, 5′-TGAATGGGAGCAAGGCTT TT-3′; reverse, 5′-CATTGCATACTGCCCGTCAA-3′), and GAPDH (forward, 5′-CCACTCTTCCACCTTCGATG-3′; reverse, 5′-TCCACCACCCTGTTGCT GTA-3′).

M-mode, two-dimensional echocardiography. Transthoracic two-dimensional echocardiography was performed using the Vevo 770 high-resolution imaging system equipped with a 30-MHz probe (Visual Sonics) in anesthetized (2% inhaled isoflurane) WT and PG CKO mice. Left ventricular (LV) wall thickness and dimension were measured from M-mode images at the plane bisecting the papillary muscles. Values were obtained by averaging three consecutive cardiac cycles, and ventricular fraction shortening (FS) and ejection fraction (EF) were calculated.

Western blotting. For Western blotting, hearts were homogenized in a modified radioimmunoprecipitation assay (RIPA) buffer (50 mM Tris-HCl [pH 7.5], 150 mM NaCl, 1 mM EDTA [pH 8.0], 1% NP-40, 0.5% Na deoxycholate, 0.1% sodium dodecyl sulfate [SDS]) containing protease inhibitors and phosphatase inhibitor cocktails I and II (Roche Diagnostics) and centrifuged at 12,000 × *g* for 15 min. The remaining Western blotting conditions were described previously (26). Western blot analyses were performed with antibodies to N-cadherin (3B9; Invitrogen), β-catenin (14; BD Biosciences), β-catenin (CAT-5H10; Invitrogen), activated β-catenin (ABC; 8E7; Millipore), αE-catenin (C2081; Sigma), αT-catenin (a kind gift from Frans van Roy, Ghent University, Ghent, Belgium), plakoglobin (15; BD Biosciences), DP (multiepitope cocktail; ARP), desmoglein-2 (a kind gift from My Mahoney, Thomas Jefferson University), plakophilin-2 (2a plus 2b; Fitzgerald), Cx43 (C6219; Sigma), GSK-3 (4G-1E; Millipore), phospho-GSK-3α/β (Ser21/9; Cell Signaling), phospho-AKT (Ser473; D9E; Cell Signaling), and AKT (pan; 40D4; Cell Signaling). For normalization of signals, blotting was also performed with an anti-GAPDH (6C5; RDI) monoclonal antibody, followed by blotting with an IRDye 680- or IRDye 800CW-conjugated secondary antibody (LI-COR). Membranes were imaged with the Odyssey infrared imaging system (LI-COR), and quantitative densitometric analysis was performed by applying Odyssey version 1.2 infrared imaging software.

Enzyme-linked immunosorbent assay (ELISA). Hearts were homogenized in a modified RIPA buffer as described above. Protein levels were assessed by using kits for mouse tumor necrosis factor alpha (TNF-α), interleukin-6 (IL-6), and IL-1β (Quantikine; R&D Systems) according to the manufacturer's instructions. Optical density was measured at 450 nm with wavelength correction at 570 nm using a plate reader (Molecular Devices). Cytokine concentrations were calculated by four-parameter regression curve fitting, and results were expressed as picograms of target protein per milligram of protein.

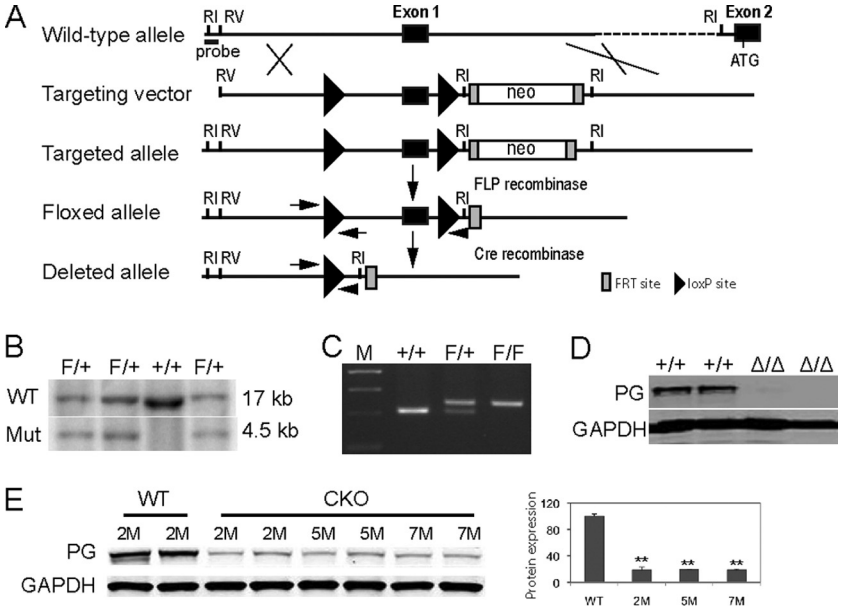

FIG. 1. Generation of a conditional *PG* mutation. (A) Schematic representation of the expected gene replacement at the *PG* locus. *loxP* sites are represented by triangles. The rectangles represent FRT sites. (B) Southern blot analysis of WT (lane 3) and targeted ES cells (lanes 1, 2, and 4). The flanking probe used for screening ES cell clones is shown (probe). After digestion with EcoRI, the WT and targeted alleles result in 17- and 4.5-kb fragments, respectively. (C) PCR analysis confirming the presence of the *loxP* sites. (D) Western blot analysis of 12.5-day-old embryo lysates demonstrating the absence of PG protein in PG null embryos (Δ/Δ). (E) Western blot analysis of heart lysates from PG CKO mice at different times after administration of Tam. ATG, initiator methionine. Restriction endonuclease sites: RI, EcoRI; RV, EcoRV. M, months; Mut, mutant. **, $P < 0.01$.

Immunofluorescence assay and immunohistochemical analysis. Hearts were isolated and fixed in 4% paraformaldehyde, dehydrated, and embedded in paraffin. Sections (6 μm) were cut, mounted, dewaxed in xylene, rehydrated through an ethanol series, and then heated in 1× Antigen Unmasking Solution (Vector Laboratories) in a microwave oven (350 W) for 10 min to unmask the epitope. Following blocking with 5% nonfat milk–PBS for 30 min, sections were incubated at 4°C for 16 h with primary antibodies diluted in 5% nonfat milk–PBS. The primary antibodies used are described above. After washing in PBS, sections were incubated with Alexa Fluor 488- or 555-conjugated goat anti-mouse or -rabbit antibody (Molecular Probes, Invitrogen) for 1 h at room temperature. After washing in PBS, sections were mounted using ProLong Gold antifade reagent containing 4′,6-diamidino-2-phenylindole (DAPI). Slides were dried overnight and imaged using a Zeiss LSM 510 META confocal microscope system.

For immunohistochemical analysis, paraffin sections were prepared as described above. After 1× Antigen Unmasking Solution (Vector Laboratories) treatment, sections were incubated for 30 min in 0.3% H_2O_2 in methanol. Sections were blocked for 30 min with diluted normal blocking serum and incubated overnight with the following primary antibodies: mouse anti-β-catenin (14; BD Transduction), mouse anti-ABC (8E7; Millipore), and rat anti-mouse macrophages/monocytes (MOMA-2, MCA519GT; ABD Serotec). For MOMA-2 staining, after incubation with rabbit biotinylated anti-rat IgG (Vector) for 30 min, sections were incubated with VECTAIN Elite ABC regent (Vector). For β-catenin staining, sections were incubated with anti-mouse EnVision+ System horseradish peroxidase-labeled polymer (DakoCytomation) for 30 min at room temperature. After washing, sections were developed in peroxidase substrate (3,3′-diaminobenzidine; Vector), counterstained with hematoxylin (Gill's Formula; Vector), cleared, and mounted. Samples were analyzed under a Nikon ECLIPSE 80i microscope.

Arrhythmia induction studies. Adult mice were heparinized (0.5 U/g intraperitoneally) and then anesthetized with 2,2,2-tribromoethanol (Avertin; 100 mg/kg intraperitoneally). The hearts were quickly removed through a thoracotomy and rinsed in Tyrode's solution containing 130 mmol/liter NaCl, 24 mmol/liter $NaHCO_3$, 1.2 mmol/liter NaH_2PO_4, 1.0 mmol/liter $MgCl_2$, 5.6 mmol/liter glucose, 4.0 mmol/liter KCl, and 1.8 mmol/liter $CaCl_2$ and equilibrated with a 95% O_2–5% CO_2 gas mixture. Hearts were then rapidly, cannulated, perfused in a retrograde fashion via an aortic cannula with 37°C oxygenated Tyrode's solution (2 to 3 ml/min), and placed in a chamber. The solution in the chamber was used as a volume conductor for recording electrocardiograms (ECGs). ECGs were recorded with a Cyber Amp380 amplifier (Axon Instruments) and digitized at 10 kHz with a Digidata 1400A and AxoScope 10.2 after equilibration for 20 min. Bipolar pacing electrodes were placed on the epicardium of the ventricle. The ventricle was paced using pulses equivalent to a 1.5× threshold amplitude with a 2-ms duration.

Transmission electron microscopy (TEM). Hearts were isolated and cannulated on a perfusion apparatus. Hearts were then pretreated in relaxation medium containing 100 mM KCl and fixed in 2% glutaraldehyde–1% paraformaldehyde in 0.08 M cacodylate buffer with 2 mM $CaCl_2$, pH 7.4, and processed for sectioning (70 nm) for TEM (JEOL JEM1010).

Coimmunoprecipitation (IP) from whole heart tissue. Heart lysates were prepared as described for Western blotting. Samples (3 mg) of lysates were precleared using TrueBlot anti-rabbit Ig IP beads (eBioscience) for 1 h at 4°C with rotation. After the beads were discarded, lysates were incubated for 60 min at 4°C with rotation with 5 μg of rabbit anti-TCF-4 (C48H11; Cell Signaling) or rabbit anti-αE-catenin (C2081; Sigma). TrueBlot anti-rabbit Ig IP beads (50 μl) were added to each reaction mixture, and the tubes were rotated further overnight at 4°C. Beads were washed four times for 5 min each time with 1 ml RIPA buffer on ice and once with 1 ml 1× PBS. Proteins were eluted from beads in 25 μl 2× NuPAGE sample buffer and subjected to SDS-polyacrylamide gel electrophoresis and Western blotting with the antibodies described above and mouse anti-TCF-4 antibody (Cell Signaling).

Statistics. Data are expressed as the mean ± the standard error of the mean (SEM). Comparisons between groups were performed with a two-tailed Student *t* test using Microsoft Excel software. Survival analysis was performed by the Kaplan-Meier method, and between-group differences in survival were tested by the log rank test. A *P* value of <0.05 was considered statistically significant.

RESULTS

Generation and characterization of PG CKO mice. Conventional gene-targeting deletion of *PG* (*JUP*) results in embryonic lethality (6, 40), preventing analysis of PG function in adult disease-related processes such as ARVC. To overcome this limitation, Cre/*loxP* technology was used to inactive the *PG* gene (Fig. 1A and B) specifically in the hearts of adult mice. The targeting vector was designed to introduce *loxP* sites

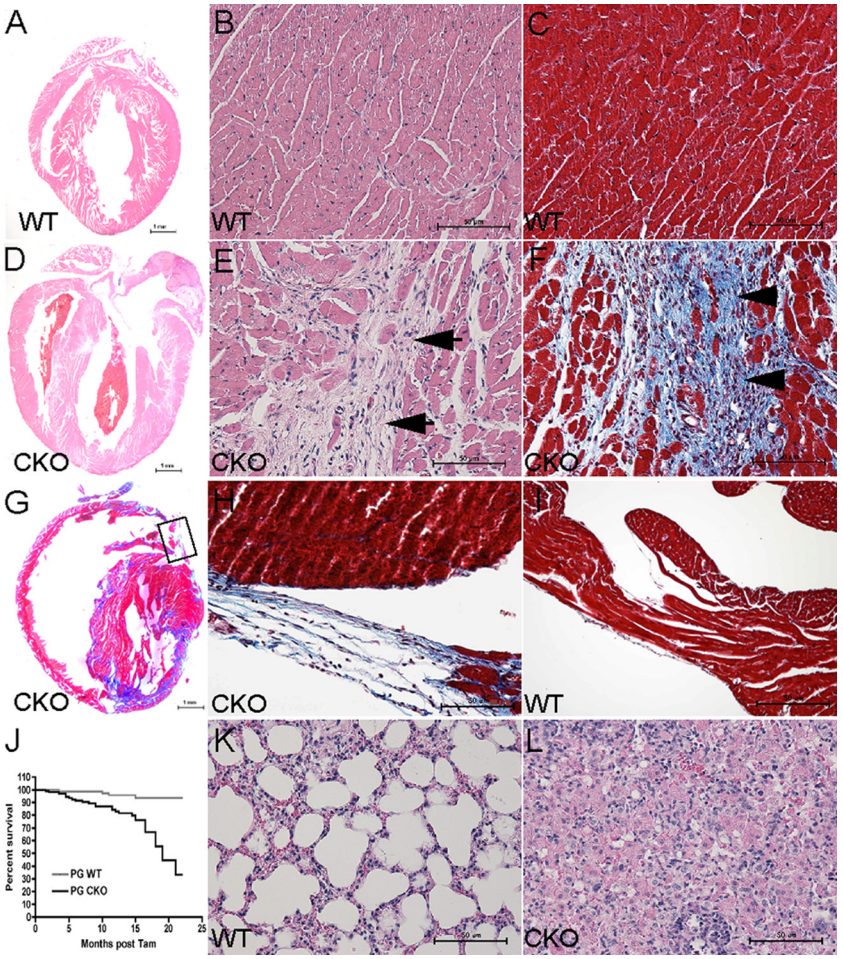

FIG. 2. Histological analysis of PG CKO mice. Heart and lung sections from $PG^{flox/flox}/Cre^{-}$ (WT) or $PG^{flox/flox}/Cre^{+}$ (CKO) mice 5 months (A to F), 9 months (G to I), or 12 months (K and L) after administration of Tam were H&E (A, B, D, E, K, and L) or Masson's trichrome (C and F to I) stained. Note the dilated ventricles (D), loss of cardiac myocytes in the myocardium (E), thin right ventricular free wall (boxed area in panel G, higher magnification in panel H), and increased fibrosis (F, G, and H) in the CKO heart compared with the WT heart. Abnormal lung histology indicative of pulmonary edema (L). (J) Kaplan-Meier survival curve following cardiac tissue-specific depletion of PG. Survival curves were carried out to 22 months after administration of Tam (WT $n = 81$, CKO $n = 105$, $P < 0.0001$ by log rank test).

around exon 1, which contains the *PG* gene transcriptional regulatory sequences. The WT and *PG* floxed alleles were distinguished by PCR analysis (Fig, 1C). To confirm that Cre recombinase would mediate deletion of the promoter and exon 1, generating a null allele, $PG^{flox/+}$ mice were initially bred to protamine/Cre transgenic mice to create a germ line mutation (34). Mice heterozygous for the *PG* mutation were intercrossed, and embryos were collected at midgestation. Western blot analysis of embryo lysates confirmed that the *PG* mutation resulted in a null allele and embryonic lethality, as previously reported (6, 40) (Fig. 1D).

The $PG^{flox/flox}$ mice were mated with α-MHC/MerCreMer transgenic mice (44) to generate a PG CKO in the adult myocardium after Tam administration. $PG^{flox/flox}$ littermates (6 to 8 weeks old) with and without the Cre transgene were given Tam for 5 consecutive days. Western analysis of heart lysates demonstrated a significant decrease in PG (-81%, $P < 0.01$) as early as 2 months after administration of Tam (Fig. 1E). Histological analysis demonstrated enlarged right and left ventricles of PG CKO mice about 5 months after administration of Tam compared with those of age-matched WT littermates (Fig. 2A and D). Consistent with human ARVC pathology, focal areas of myocyte loss and replacement by fibrous tissue, along with patchy inflammatory infiltrates, were revealed in the myocardium of PG CKO hearts beginning at about 2 months after administration of Tam (Fig. 2; see Fig. S1 in the supplemental material). Progressive thinning of the right ventricular free wall was observed in the PG CKO animals (Fig. 2). Terminal deoxynucleotidyltransferase-mediated dUTP-biotin nick end labeling analysis (see Fig. S1 in the supplemental material) showed increased apoptotic cells in PG CKO hearts at 5 months after administration of Tam (3.7% for CKO versus 0.01% for WT, $P < 0.01$, $n = 4$). The apoptotic cells were observed in areas close to myocyte loss and fibrous tissue replacement. ARVC patients exhibit replacement of cardiomyocytes with adipocytes; however, adipocytes were not observed in regions of myocyte loss and Oil Red O staining did not detect a significant increase in lipid accumulation in the PG CKO model (data not shown). Cardiac death occurred in 24.8% of the PG CKO mice (26/105 $PG^{flox/flox}/Cre^{+}$), com-

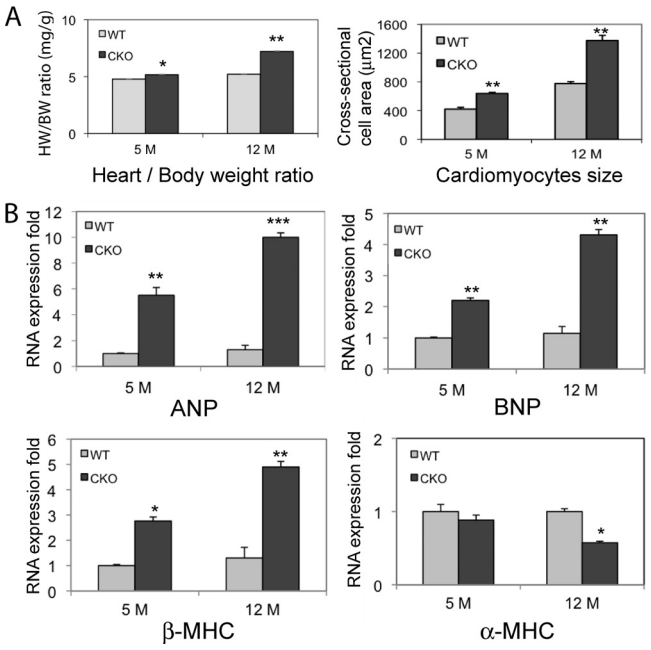

FIG. 3. Characterization of the hypertrophic response of PG CKO hearts. (A) Quantification of heart weight/body weight ratios of $PG^{flox/flox}/Cre^{-}$ (WT) and $PG^{flox/flox}/Cre^{+}$ (CKO) mice at 5 and 12 months (M) after administration of Tam ($n = 20$ from each group) and quantification of the myocyte cross-sectional area from cardiac histological sections of $PG^{flox/flox}/Cre^{-}$ (WT) and $PG^{flox/flox}/Cre^{+}$ (CKO) hearts at 5 and 12 months after administration of Tam ($n = \geq 100$ cells from at least three different animals per group). (B) Quantification of mRNA expression from $PG^{flox/flox}/Cre^{-}$ (WT) and $PG^{flox/flox}/Cre^{+}$ (CKO) hearts at 5 and 12 months after administration of Tam for ANP, BNP, β-MHC, and α-MHC ($n = 8$ to 12 mice from the 5-month group and 3 mice from the 12-month group). Note the marked fetal gene program activation at 5 and 12 months (ANP, BNP, and β-MHC) and the decreased level of the differentiated myocyte marker α-MHC at 12 months after administration of Tam in CKO hearts (*, $P < 0.05$; **, $P < 0.01$; ***, $P < 0.001$).

pared with only 4.9% of their WT littermates (4/81 $PG^{flox/flox}/Cre^{-}$; $\chi^2 = 15.1$, $P < 0.0001$) beginning at 3 months after administration of Tam (Fig. 2J). Signs of heart failure such as lung edema (Fig. 2K and L) and animal inactivity were observed in older PG CKO mice (9 to 12 months after administration of Tam). These data indicated that deletion of PG specifically from the heart caused myocyte loss, fibrous tissue replacement, and myocardial wall thinning, which are typical pathological features of ARVC.

With increasing age, the PG CKO animals displayed increased heart weight/body weight ratios and cardiomyocyte cross-sectional areas (Fig. 3A). Analysis of hypertrophic/stress-responsive genes by real-time PCR analysis showed increased ANP, BNP, and β-MHC gene expression in PG CKO hearts at 5 and 12 months after administration of Tam compared with those of WT littermates (Fig. 3B). Furthermore, the differentiation marker α-MHC was decreased at 12 months after administration of Tam (Fig. 3B).

Increased production of proinflammatory cytokines in PG CKO mice. Inflammation is seen in up to 75% of the hearts of ARVC patients at autopsy (46). To evaluate the inflammatory phenotype in PG CKO mice, we performed immunohistochemical analysis staining for activated macrophages/monocytes in the myocardium of PG CKO hearts. The MOMA-2-positive macrophages/monocytes adjacent to dying and damaged myocytes were remarkably increased within the ventricular wall lesion area of massive myocyte loss in PG CKO compared with WT hearts at 5 months after administration of Tam (Fig. 4A and B). Neutrophil infiltrates in the myocardium of the PG CKO mice were also evident by histological staining (Fig. 4C). Since macrophages and neutrophils are major sources of proinflammatory cytokines, we performed ELISAs of heart lysates to examine the expression of IL-6, IL-1β, and TNF-α in PG CKO mice and control littermates. Interestingly, IL-6 and IL-1β, but not TNF-α, were upregulated in PG CKO

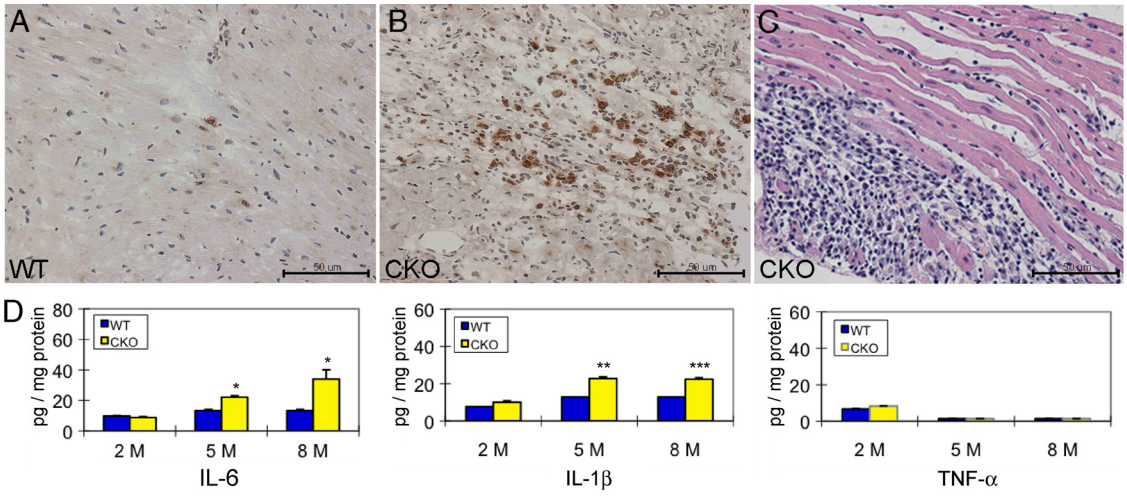

FIG. 4. Increased inflammatory response in PG CKO hearts. Heart sections from $PG^{flox/flox}/Cre^{-}$ (WT, A) and $PG^{flox/flox}/Cre^{+}$ (CKO, B) mice at 5 months after administration of Tam were immunostained for the activated macrophage/monocyte marker MOMA-2. MOMA-2-positive macrophages were observed in areas with myocyte loss in CKO hearts (B), in contrast to WT hearts (A). (C) High magnification of H&E staining in the myocardium showed marked increased inflammatory cells from a CKO heart at 5 months after administration of Tam. (D) Heart lysates from $PG^{flox/flox}/Cre^{-}$ (WT) and $PG^{flox/flox}/Cre^{+}$ (CKO) mice after administration of Tam were examined by ELISA for the proinflammatory cytokines IL-6, IL-1β, and TNF-α ($n = 20$ from each group). Note the elevated IL-6 and IL-1β, but not TNF-α, levels in the CKO hearts at 5 and 8 months compared with those in WT hearts (*, $P < 0.05$; **, $P < 0.01$; ***, $P < 0.001$).

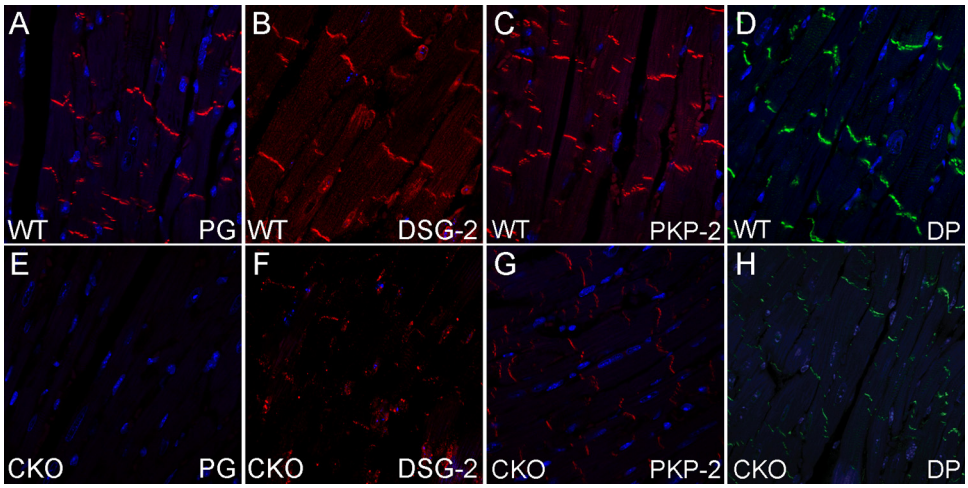

FIG. 5. ICD expression of desmosomal proteins in PG CKO hearts. Heart sections from $PG^{flox/flox}/Cre^{-}$ (A to D) and $PG^{flox/flox}/Cre^{+}$ (E to H) mice at 5 months after administration of Tam were immunostained for PG (A and E), DSG-2 (B and F), PKP-2 (C and G), and DP (D and H). Note the decreased ICD expression of PG, DSG-2, PKP-2, and DP in CKO hearts compared with that in WT hearts.

hearts at 5 and 8 months after administration of Tam (Fig. 4D). The increase in cytokine expression was associated with the severity of myocyte loss in PG CKO hearts, as no change was observed at 2 months after administration of Tam before significant myocardial injury was observed (see Fig. S1 in the supplemental material). These results demonstrated that cardiac tissue-specific loss of PG led to myocyte loss accompanied by an inflammatory response, with macrophages likely providing a source of local cytokine production besides stressed cardiac myocytes.

Remodeling of ICD in PG-depleted hearts. Cardiomyocytes are interconnected by the ICD structure, which consists of three main junctional complexes: desmosomes, adherens junctions, and gap junctions. PG is the only ICD component common to both desmosomes and adherens junctions. It can bind to a large number of adhesion proteins located at the ICD, including DSG-2, DSC-2, DP, PKP-2, N-cadherin, and α-catenins (16). To examine the effect of PG depletion on the expression of ICD proteins, we performed immunofluorescence assays of PG CKO hearts at 5 months after administration of Tam. Representative images of the ventricular myocardium are shown. The strong PG staining normally found in the ICD was absent in PG CKO heart tissue, in contrast to WT heart tissue (Fig. 5A and E). The PG-binding proteins DSG-2 (Fig. 5B and F), PKP-2 (Fig. 5C and G), and DP (Fig. 5D and H) were remarkably reduced at the ICD in PG CKO hearts. In contrast, the adherens junction proteins N-cadherin (Fig. 6A and C), αE-catenin, and αT-catenin (data not shown) remained localized at the ICD in PG CKO hearts. Western analysis detected a modest decrease in total PKP-2 levels (-28%, $P < 0.05$), whereas the total protein levels of the other desmosomal components were not significantly changed in PG CKO hearts (data not shown). Taken together, these data indicate that loss of PG primarily affects the localization of desmosomal proteins to the ICD.

The irregular heart rhythms experienced by ARVC patients are thought to be due to conduction abnormalities caused by gap junction remodeling. Therefore, we examined the expression and distribution of the gap junction protein Cx43 in PG CKO mice. Cx43-containing gap junction plaques were reduced at the ICD in PG CKO hearts (Fig. 6B and D), consistent with decreased expression of Cx43 in ARVC patients (2, 21, 22). However, electrophysiological analysis using volumetric ECG recordings did not detect a significant change in the PR (41.5 ± 2.1 ms [$n = 12$, CKO] versus 42.4 ± 2.9 ms [$n = 6$, WT]) or QRS (15.6 ± 3.8 ms [$n = 12$, CKO] versus 16.4 ± 1.4 ms [$n = 6$, WT]) interval, suggesting no apparent conduction abnormality in the PG CKO mice. To determine whether the animals were susceptible to induced arrhythmias, ventricular programmed electrical stimulation of the heart was performed. Burst ventricular pacing at a cycle length of 50 ms did not induce arrhythmias in PG CKO (0/12) or WT (0/6) hearts. In contrast, arrhythmias were induced in N-cadherin$^{-/+}$

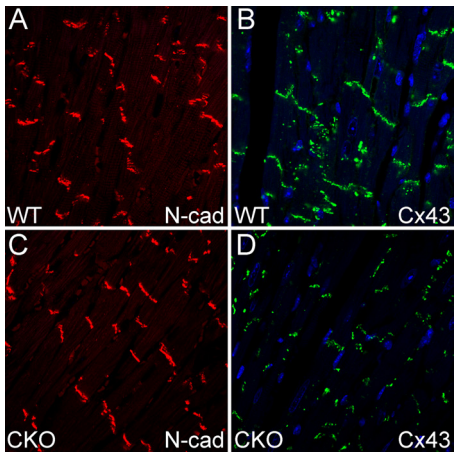

FIG. 6. ICD expression of the adherens junction protein N-cadherin (N-cad) and the gap junction protein Cx43 in PG CKO hearts. Heart sections from $PG^{flox/flox}/Cre^{-}$ (A and B) and $PG^{flox/flox}/Cre^{+}$ (C and D) mice at 5 months after administration of Tam were immunostained for N-cadherin (A and C) and Cx43 (B and D). Note the decreased expression of Cx43 at the ICD.

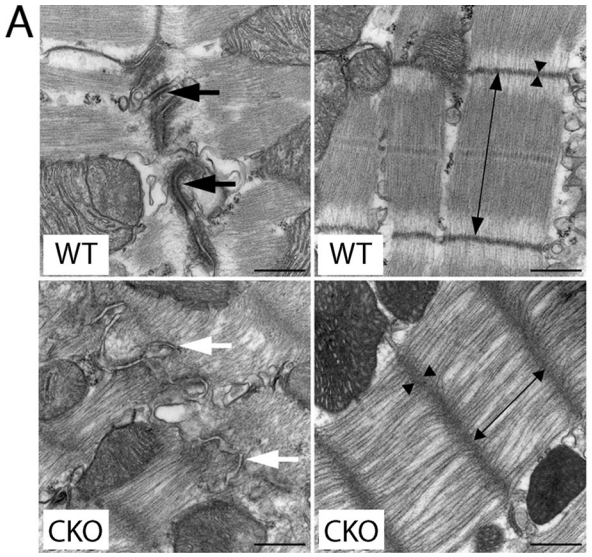

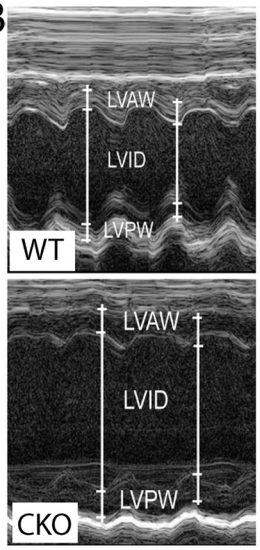

Echocardiographic indices of cardiac size and function

	WT	CKO	p
n	11	11	NA
Gender (M/F)	8/3	8/3	NA
Age (mo)	7	7	NA
Post Tam (mo)	5	5	NA
Body weight (g)	28.62 ± 0.33	31.48 ± o.41	p>0.05
Heart rate (bpm)	452.82 ± 5.4	453.55 ± 7.11	p>0.05
LVID;s (mm)	2.78 ± 0.04	3.38 ± 0.05	p<0.01
LVID;d (mm)	3.87 ± 0.05	4.34 ± 0.05	p<0.05
LV vol;s (mm)	30.61 ± 1.05	48.25 ± 1.66	p<0.01
LV vol;d (mm)	65.74 ± 1.72	86.42 ± 2.41	p<0.05
EF (%)	55.64 ± 0.64	44.71 ± 0.77	p<0.01
FS (%)	28.65 ± 0.41	22.17 ± 0.66	p<0.01
LVPW;d (mm)	0.55 ± 0.00	0.66 ± 0.01	p<0.05
LVPW;s (mm)	0.78 ± 0.02	0.89 ± 0.02	p>0.05
LVAW;d (mm)	0.71 ± 0.02	0.77 ± 0.01	p>0.05
LVAW;s (mm)	0.83 ± 0.02	0.83 ± 0.02	p>0.05

Values are means ± SEM; n, no. of mice. LVID;s,left ventricular internal dimension; LV vol, left ventricular volume; EF, ejection fraction; FS, fraction shortening; LVPW, left ventricular posterior wall; LVAW, left ventricular anterior wall; d, diastole; s, systole. p values were determined by 2-tailed Student's t test.

FIG. 7. Ultrastructural and cardiac function studies of PG CKO mice. (A) TEM of PG CKO hearts. Electron micrographs of LV myocardium from $PG^{flox/flox}/Cre^{-}$ (WT) and $PG^{flox/flox}/Cre^{+}$ (CKO) mouse hearts at 3 months after administration of Tam. Fewer and less electron-dense desmosomes (white arrow) were observed in CKO than in WT hearts (black arrows). The myofibrils appeared distorted in the CKO compared with those of the WT, with decreased sarcomere length (double-headed arrow) and wider, less dense Z lines (arrowheads). Bars, 500 nm. (B) Echocardiographic assessment of cardiac function in PG CKO mice at 5 months after administration of Tam. Shown is M-mode two-dimensional echocardiography displaying LV chamber dilation in mutant mice. Mean values of echocardiographic parameters from WT and CKO mice. Data represent the mean ± SEM. A P value of <0.05 was considered statistically significant. Note the significantly increased LV end-systolic and -diastolic internal dimension (LVID) and volume (LV vol) and reduced LV EF and FS in PG CKO mice. NA, not applicable; M/F, male/female; bpm, beats per minute.

$Cx43^{-/+}$ hearts (3/4) as previously reported (25), confirming the effectiveness of the stimulation protocol. These data suggest that the PG CKO model may not recapitulate the arrhythmogenic phenotype observed in ARVC patients.

To examine myocyte cell-cell interactions at the ultrastructural level, TEM of PG CKO ($n = 3$) and WT ($n = 2$) hearts was performed at 3 months after administration of Tam. The morphology of the ICD was grossly altered, as typical electron-dense desmosome structures were absent in PG CKO hearts (Fig. 7A). Instead, adherens-type junctions with less submembranous electron-dense material were prominently seen in PG CKO hearts (Fig. 7A). Quantitative analysis of TEM images demonstrated a significant reduction in the number (23.55 ± 13.42 [CKO] versus 45.98 ± 32.87 [WT] per 100-μm ICD; $n = 10$ fields per heart; $P < 0.001$) and length (0.14 ± 0.12 [CKO] versus 0.24 ± 0.10 [WT] per 100-μm ICD; $n = 10$ fields per heart; $P < 0.01$) of desmosomes, whereas the number (85.87 ± 32.37 [CKO] versus 54.93 ± 29.29 [WT] per 100-μm ICD; $n = 10$ fields per heart; $P < 0.01$) and length (0.30 ± 0.15 [CKO] versus 0.23 ± 0.06 [WT] per 100-μm ICD; $n = 10$ fields per heart; $P < 0.05$) of adherens junctions were increased at the ICD of the PG CKO hearts. The sarcomeres appeared distorted and compressed compared with those of WT mice (Fig. 7A), with decreased sarcomere length (1,200.91 [CKO] ± 125.12 nm versus 1,686.01 ± 123.39 nm [WT]; $n = 10$ fields per heart; $P < 0.001$) and wider, less dense Z lines (78.96 ± 22.32 nm [CKO] versus 60.86 ± 8.82 nm [WT]; $n = 10$ fields per heart; $P < 0.001$). The sarcomere defects in the PG CKO myocardium, which presumably reflect altered myofibril anchorage at the plasma membrane, suggest that PG and the desmosome play a critical role in stabilizing myofibrils.

To assess cardiac function, M-mode and two-dimensional echocardiography of PG CKO and control mice was performed at 5 months after administration of Tam (Fig. 7B). Quantitative analysis of image data demonstrated increases in the LV end-systolic and -diastolic internal dimension (LVID) and volume (LV vol) in PG CKO hearts compared with those of WT hearts (Fig. 7B). Both the LV EF and FS were reduced in PG CKO mice. LV systolic posterior wall (LVPW; s) thickness was moderately increased in CKO mice. LV diastolic posterior wall (LVPW; d) thickness and LV anterior wall (LVAW) thickness were comparable between groups (Fig. 7B). Echocardiographic measurements demonstrated that PG CKO animals exhibited modest ventricular dilation, mild LV hypertrophy, and impaired cardiac function, consistent with PG's structural role in the heart.

Activation of β-catenin signaling in PG CKO hearts. Recent evidence suggests that the pathogenesis of ARVC is related to both desmosome structural defects and alteration of β-catenin signaling (15, 27). In addition to PG's adhesive function, it can also modulate Wnt/β-catenin signaling by competing with β-catenin for binding to the transcriptional coactivator TCF/LEF. The cytosolic levels of β-catenin are tightly regulated by the GSK/axin/APC degradation complex, thus limiting β-catenin's ability to interact with TCF/LEF and activate target genes. Interestingly, β-catenin, a PG homolog, was significantly increased in PG CKO hearts (+153% versus controls; $P < 0.001$; $n = 4$ or 5) (Fig. 8A). In addition to the increased β-catenin at the ICD, cytosolic β-catenin was observed heterogeneously throughout the myocardium of PG CKO mice (Fig. 8B). To determine whether β-catenin expression was affected at the mRNA level, real-time PCR analysis of PG CKO hearts was performed. β-Catenin mRNA levels did not change after PG deletion, indicating that posttranscriptional regulation was

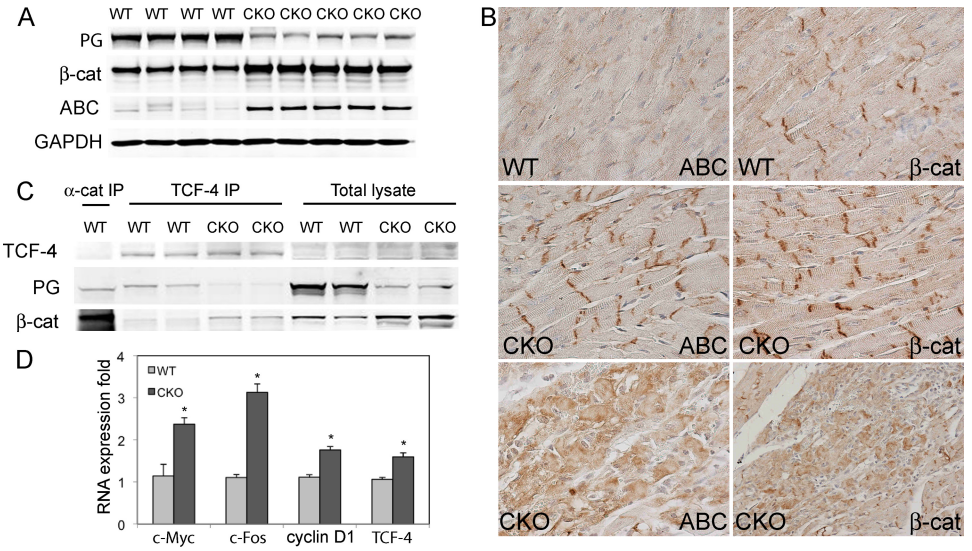

FIG. 8. β-Catenin expression and signaling in PG CKO mouse hearts. (A) Heart lysates from $PG^{flox/flox}/Cre^{-}$ (WT) and $PG^{flox/flox}/Cre^{+}$ (CKO) mice at 5 months after administration of Tam were blotted for PG, β-catenin (β-cat), and ABC. Note the significantly increased β-catenin and ABC protein levels in the CKO hearts ($n = 4$ or 5 from each group). (B) Heart sections from $PG^{flox/flox}/Cre^{-}$ (WT) and $PG^{flox/flox}/Cre^{+}$ (CKO) mice at 5 months after administration of Tam were immunostained for ABC and β-catenin. Increased ICD and cytoplasmic staining of ABC and β-catenin was observed in CKO hearts compared with that in WT hearts. (C) Heart lysates from $PG^{flox/flox}/Cre^{-}$ (WT) and $PG^{flox/flox}/Cre^{+}$ (CKO) mice at 5 months after administration of Tam were immunoprecipitated (IP) with anti-TCF-4 antibody and then blotted for PG and β-catenin. Anti-α-catenin (α-cat) antibody was used as a positive control for IP. Note that PG was the primary binding partner of TCF-4 in WT hearts. In the absence of PG, β-catenin was complexed with TCF-4. (D) Real-time PCR demonstrated an increase in β-catenin/TCF-4 target genes c-*Myc*, c-*Fos*, *cyclin D1*, and *TCF-4* in the PG CKO compared to those in the WT at 5 months after administration of Tam ($n = 8$ to 12 from each group). The results are expressed as arbitrary fold increases relative to the WT level. (*, $P < 0.05$).

responsible for the upregulation of β-catenin (data not shown). It is well known that when β-catenin is unphosphorylated at Ser33, Ser37, and Thr41, it is more stable and transcriptionally active than forms of β-catenin phosphorylated at these sites (17, 29, 45). We took advantage of an antibody recently developed that only recognizes the dephosphorylated epitopes of β-catenin (29) to characterize the regulation of stabilized β-catenin or ABC in PG CKO hearts. Remarkably, Western analysis showed a 9.8-fold increase in the activated β-catenin/total β-catenin ratio in PG CKO hearts ($P < 0.001$, $n = 4$ or 5, Fig. 8A), indicating a significant change in β-catenin regulation in the absence of PG. β-Catenin regulation was perturbed in PG CKO mice as early as 2 months after administration of Tam (data not shown). Immunohistochemical analysis revealed cytoplasmic and ICD localization of activated β-catenin in PG CKO hearts compared to relatively low expression in WT hearts (Fig. 8B). To determine if stabilized β-catenin resulted in increased interaction with the TCF/LEF transcription factor, coimmunoprecipitation was performed with anti-TCF-4 antibody and probed for PG and β-catenin. In WT hearts, PG was the primary binding partner of TCF-4; however, when PG was ablated, β-catenin became associated with TCF-4, demonstrating that PG directly competes with β-catenin for TCF-4 binding (Fig. 8C). To determine if the increased association of β-catenin with TCF-4 in PG CKO hearts resulted in increased transcription of β-catenin target genes, quantitative real-time PCR analysis of heart samples was performed. Several β-catenin/TCF/LEF target genes (c-*Myc*, c-*Fos*, *cyclin D1*, and *TCF-4*) were upregulated in PG CKO hearts (Fig. 8D). Other β-catenin target genes, *axin-2* and *Cx43*, were unchanged in PG CKO hearts (data not shown). Among the four target genes upregulated, c-MYC protein levels were increased in PG-deficient cardiomyocytes (data not shown). Taken together, these data demonstrate that PG interferes with β-catenin transcriptional activity by competing for TCF-4 binding, consistent with an antagonistic role for PG in β-catenin-mediated signaling.

The kinase GSK-3 is responsible for the phosphorylation of β-catenin, thus targeting it for degradation via the proteosome. To determine the mechanism responsible for β-catenin stabilization, GSK-3 activity was examined in PG CKO hearts. Two isoforms of GSK-3 are expressed in the heart which are inactive when phosphorylated at Ser21 (pSer21-GSK-3α) and Ser9 (pSer9-GSK-3β), thus leading to increased cytosolic β-catenin levels. A significant increase in GSK-3β phosphorylated forms relative to total GSK-3β was observed in PG CKO hearts at 5 to 8 months after administration of Tam (Fig. 9), consistent with inhibition of GSK-3β activity leading to an increased level of β-catenin dephosphorylated at its N-terminal serine and threonine residues (Fig. 8A).

It is well established that the primary mechanism of inhibiting GSK-3α/β activity is phosphorylation of its amino-terminal serine residue via activated PKB/AKT (8). To determine whether PKB/AKT activity was increased in PG CKO hearts, we performed a Western blot assay using a phospho-specific PKB/AKT antibody. Coincident with the increase in phosphorylation of GSK-3β at Ser9 in the PG CKO heart, active PKB/AKT, as evidenced by Ser473 phosphorylation, was identified in PG CKO hearts (Fig. 9). In addition, PKB/AKT can directly phosphorylate β-catenin at Ser552, causing its disassociation from cell-cell contacts and accumulation in both the cytosol

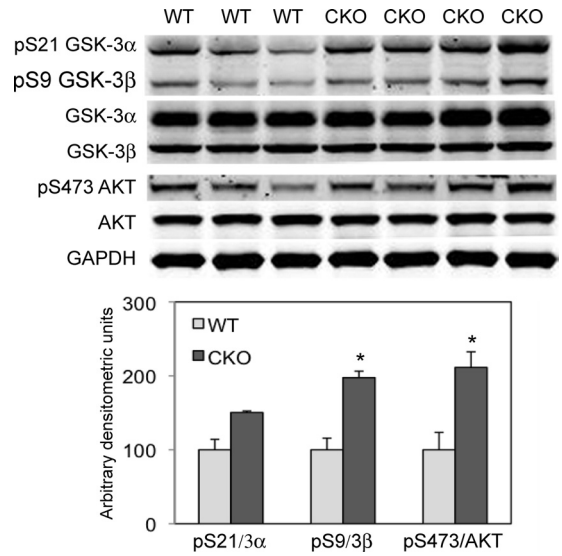

FIG. 9. Depletion of PG led to activation of AKT and inhibition of GSK-3β. Heart lysates from $PG^{flox/flox}/Cre^{-}$ (WT) and $PG^{flox/flox}/Cre^{+}$ (CKO) mice at 5 to 8 months after administration of Tam were blotted for pSer21-GSK-3α, pSer9-GSK-3β, GSK-3α/β, pSer473-AKT, and AKT ($n = 5$ or 6 from each group). Note the markedly increased expression of pSer9-GSK-3β and pSer473-AKT in CKO hearts compared with that in WT hearts (*, $P < 0.05$).

and the nucleus (13). An increase in pS552-β-catenin was observed in PG CKO hearts, consistent with its accumulation in the cytosol (data not shown). Taken together, these results suggest that stabilization of β-catenin following loss of PG may be due to activation of PKB/AKT and its ability to directly and indirectly affect β-catenin phosphorylation via inactivation of GSK-3β.

DISCUSSION

ARVC is considered a disease of the desmosome, as about half of the mutations identified are found in genes encoding desmosomal proteins, including PG (10). Germ line deletion of the *PG* (*JUP*) gene results in embryonic lethality in mice (6, 40); therefore, a CKO is required to investigate PG's role in ARVC. We show that replacement of the ventricular myocardium by fibrous tissue is progressive in PG CKO mice, starting from the midmyocardium and extending transmurally, leading to ventricular wall thinning. Myocardial loss was the consequence of cell death initiated by apoptosis and followed by myocytolysis, inflammatory infiltrates, and myocardial atrophy. The presence of replacement-type fibrosis and myocyte degenerative changes in the PG CKO fulfilled the requirement of a histological diagnosis of ARVC (30).

The inability to induce arrhythmias was unexpected, given the decrease in Cx43-containing gap junction plaques in PG CKO hearts. Furthermore, it was reported that PG heterozygous animals are susceptible to ventricular arrhythmias (23). The reason for the difference in arrhythmogenicity between the two models is unclear. It was previously shown that β-catenin interacts with Cx43 and enhances gap junction communication in cultured cardiomyocytes (1). Hence, the increased β-catenin at the ICD in PG CKO hearts may enhance the function of the remaining gap junctions, thus protecting the animals against arrhythmias. In ARVC patients where the PG protein is truncated at the carboxy terminus (i.e., Naxos disease), there is a high incidence of arrhythmias and no apparent change in β-catenin at the ICD (22). Additional studies are necessary to determine β-catenin's function in gap junction remodeling in the PG CKO model.

Fibrofatty tissue replacement of cardiomyocytes is observed in ARVC patients; however, we did not observe adipocytes in PG CKO hearts. Consistent with observations in the transgenic mouse ARVC model expressing the human DSG-2 dominant negative mutation N271S (36), we did not observe a significant increase in lipid droplet accumulation as determined by Oil Red O staining. The lack of overt adipocyte differentiation in the PG CKO may be due to species differences since little adipose tissue is associated with the murine heart, in contrast to the human heart. Alternatively, it is possible that PG's function as a transcriptional regulator is required for transdifferentiation of a cardiac progenitor cell into an adipocyte, as suggested by Marian and coworkers (27).

The phenotype caused by loss of PG in the heart is unique and different from that caused by deleting genes encoding the adherens junction components N-cadherin (24), αE-catenin (43), and β-catenin (49) in mice. Both N-cadherin and αE-catenin CKO models exhibit dilated cardiomyopathy; however, neither model causes myocyte loss with subsequent inflammation (24, 43). β-Catenin CKO mice do not develop cardiomyopathy presumably due to compensation by PG (49). In the PG CKO model, although increased at the ICD, β-catenin is not capable of compensating for loss of PG in the desmosome, leading to an altered desmosome structure. The injury response in the PG CKO and other animal models of ARVC (15, 27, 36, 48) suggests that a different signaling pathway(s) is activated after interfering with desmosomes rather than adherens junctions.

In WT adult hearts, we find that PG is primarily bound to TCF-4, consistent with the lack of transcriptional activity of β-catenin/TCF/LEF target genes. This result is consistent with the catenins' mutually exclusive pattern of interaction with their common binding partners, which include cadherins, LEF/TCF transcription factors, and the GSK-3/axin/APC degradation complex. It has been shown that transfected PG and β-catenin are both effective in coimmunoprecipitating LEF-1, and the catenin-binding domain of LEF-1 is equally potent in recruiting PG or β-catenin to the promoter region (19). In the WT adult heart in the absence of a Wnt signal, cytosolic β-catenin is tightly regulated by the GSK/axin/APC degradation complex. Indeed, activation of β-catenin signaling in the PG-depleted myocardium was an important finding in our study. This result demonstrates that, in addition to PG's structural role in desmosomes and adherens junctions, PG is a potent antagonist of β-catenin signaling in the heart. Because β-catenin lacks a DNA-binding domain, its role as a transactivator requires interaction with members of the TCF/LEF transcription factor family to mediate DNA binding and activate the transcription of β-catenin/TCF/LEF target genes. In the PG CKO, β-catenin is found complexed with TCF-4, and target genes which have been implicated in the regulation of hypertrophy, c-*Myc* and c-*Fos*, are activated (7). As transcription cofactors, both PG and β-catenin, through binding to

TCF/LEF, can either activate or suppress gene transcription, depending on the targets and cellular context (28, 33, 50, 51). For example, PG was shown to suppress the expression of c-Myc in epidermal keratinocytes in a Lef-1-dependent manner (47). Therefore, we cannot exclude the possibility that loss of PG relieves the suppression of target genes such as c-*Myc*, thus contributing to the hypertrophic phenotype of PG CKO mice.

Numerous studies of adult or terminally differentiated cardiac myocytes indicate that β-catenin/TCF/LEF targets are dominant regulators of cardiomyocyte growth (7). The prohypertrophic agents phenylephrine and endothelin 1 can stabilize β-catenin and activate a TCF/LEF reporter (18). Overexpression of a stabilized mutant form of β-catenin via adenovirus-mediated gene transfer can drive hypertrophic growth in cardiomyocytes (18). In contrast, induced deletion of β-catenin specifically from the myocardium leads to a blunted hypertrophic response to pathological stress-induced growth accompanied by reduced c-*Myc* and c-*Fos* gene expression (7). Similarly, cardiac tissue-specific haploinsufficiency of β-catenin inhibits cardiac hypertrophy in response to pressure overload (38). Furthermore, expression of a dominant inhibitory mutant form of LEF-1 in which the β-catenin-binding domain is deleted leads to a dramatic reduction in cardiomyocyte growth (7). Because β-catenin levels were elevated before apparent myocyte loss, we believe that activation of AKT and inhibition of GSK-3 followed myocardial damage and that inflammation may enhance β-catenin-mediated hypertrophy in the PG CKO model. Interestingly, a transgenic animal model of ARVC expressing the human DP dominant negative mutation R2834H showed upregulation of β-catenin, including an increase in the cytoplasmic fraction, suggesting potential activation of β-catenin target genes that could contribute to cardiac hypertrophy in ARVC (48).

Inflammation is commonly observed in the hearts of ARVC patients at autopsy (46). Furthermore, it has been reported that the serum concentration of IL-6 increases after myocardial infarction, congestive heart failure, and hypertrophic and dilated cardiomyopathy (14). IL-6 can promote myocyte hypertrophy and induce norepinephrine-mediated LV remodeling (32). IL-6/gp130-mediated signaling is involved in overload-induced cardiac hypertrophy in the rodent heart (35). Pressure-mediated hypertrophy and mechanical stretching induce IL-1 release and subsequent insulin growth factor 1 generation to maintain compensative hypertrophy by affecting the AKT and JNK pathways (20). AKT (acting downstream of phosphatidylinositol 3-kinase [PI3K]) is the major kinase regulating the inhibition of GSK-3 by phosphorylating its N-terminal serine residues (11). In the PG CKO, sustained stimulation of IL-6 and IL-1β following myocardial damage may be sufficient to induce activation of the PI3K/AKT pathway, and subsequently promote cardiac hypertrophy via β-catenin signaling.

In conclusion, our results demonstrate for the first time the dual functions of PG as a cell adhesion and signaling molecule in the working myocardium. The PG CKO model recapitulates many features of ARVC, including myocyte loss, inflammation, fibrous tissue replacement, myocardial wall thinning, and heart failure. Furthermore, the penetrance and expressivity of the phenotype was variable in the PG CKO mice similar to human ARVC patients. Finally, we show that loss of PG leads to stabilization of β-catenin resulting in increased β-catenin/TCF transcriptional activity, which may contribute to ARVC pathogenesis. This novel model of ARVC demonstrates for the first time the ability of PG to antagonize β-catenin signaling in the heart and its implications for disease pathogenesis.

ACKNOWLEDGMENTS

This work was supported by a grant from the National Institutes of Health (HL081569 to G.R.) and American Heart Association scientist development grant 2080068 (to J.L.).

We are grateful to Thomas Force, Donna Woulfe, and My Mahoney for comments. We thank Peter Koch for assistance with generating the PG targeting construct; Arnold Greenspon and Matthew Ortman for assistance with ECG measurements; Tung Chan for TNF1.6 transgenic tissue; Frans van Roy for anti-αT-catenin antibody; My Mahoney for anti-desmoglein-2 antibody; and Han Du, Craig Riley, David Kurz, Leeanne Griffith, and Andrew Ho for technical assistance. We thank Jean Richa and the University of Pennsylvania Transgenic Core Facility and Ray Meade and the University of Pennsylvania Biomedical Imaging Core Facility for electron microscopy analysis and the Jefferson Kimmel Cancer Center Bioimaging Facility for confocal imaging.

REFERENCES

1. **Ai, Z., A. Fischer, D. C. Spray, A. M. Brown, and G. I. Fishman.** 2000. Wnt-1 regulation of connexin43 in cardiac myocytes. J. Clin. Invest. **105:**161–171.
2. **Asimaki, A., et al.** 2007. A novel dominant mutation in plakoglobin causes arrhythmogenic right ventricular cardiomyopathy. Am. J. Hum. Genet. **81:** 964–973.
3. **Asimaki, A., et al.** 2009. A new diagnostic test for arrhythmogenic right ventricular cardiomyopathy. N. Engl. J. Med. **360:**1075–1084.
4. **Basso, C., D. Corrado, F. I. Marcus, A. Nava, and G. Thiene.** 2009. Arrhythmogenic right ventricular cardiomyopathy. Lancet **373:**1289–1300.
5. **Basso, C., et al.** 2006. Ultrastructural evidence of intercalated disc remodelling in arrhythmogenic right ventricular cardiomyopathy: an electron microscopy investigation on endomyocardial biopsies. Eur. Heart J. **27:**1847–1854.
6. **Bierkamp, C., K. J. McLaughlin, H. Schwarz, O. Huber, and R. Kemler.** 1996. Embryonic heart and skin defects in mice lacking plakoglobin. Dev. Biol. **180:**780–785.
7. **Chen, X., et al.** 2006. The beta-catenin/T-cell factor/lymphocyte enhancer factor signaling pathway is required for normal and stress-induced cardiac hypertrophy. Mol. Cell. Biol. **26:**4462–4473.
8. **Cross, D. A., D. R. Alessi, P. Cohen, M. Andjelkovich, and B. A. Hemmings.** 1995. Inhibition of glycogen synthase kinase-3 by insulin mediated by protein kinase B. Nature **378:**785–789.
9. **Delmar, M., and W. J. McKenna.** 2010. The cardiac desmosome and arrhythmogenic cardiomyopathies: from gene to disease. Circ. Res. **107:**700–714.
10. **den Haan, A. D., et al.** 2009. Comprehensive desmosome mutation analysis in North Americans with arrhythmogenic right ventricular dysplasia/cardiomyopathy. Circ. Cardiovasc. Genet. **2:**428–435.
11. **Dorn, G. W., II, and T. Force.** 2005. Protein kinase cascades in the regulation of cardiac hypertrophy. J. Clin. Invest. **115:**527–537.
12. **Drees, F., S. Pokutta, S. Yamada, W. J. Nelson, and W. I. Weis.** 2005. Alpha-catenin is a molecular switch that binds E-cadherin-beta-catenin and regulates actin-filament assembly. Cell **123:**903–915.
13. **Fang, D., et al.** 2007. Phosphorylation of beta-catenin by AKT promotes beta-catenin transcriptional activity. J. Biol. Chem. **282:**11221–11229.
14. **Fischer, P., and D. Hilfiker-Kleiner.** 2008. Role of gp130-mediated signalling pathways in the heart and its impact on potential therapeutic aspects. Br. J. Pharmacol. **153**(Suppl. 1)**:**S414–S427.
15. **Garcia-Gras, E., et al.** 2006. Suppression of canonical Wnt/beta-catenin signaling by nuclear plakoglobin recapitulates phenotype of arrhythmogenic right ventricular cardiomyopathy. J. Clin. Invest. **116:**2012–2021.
16. **Green, K. J., and C. A. Gaudry.** 2000. Are desmosomes more than tethers for intermediate filaments? Nat. Rev. Mol. Cell Biol. **1:**208–216.
17. **Guger, K. A., and B. M. Gumbiner.** 2000. A mode of regulation of beta-catenin signaling activity in Xenopus embryos independent of its levels. Dev. Biol. **223:**441–448.
18. **Haq, S., et al.** 2003. Stabilization of beta-catenin by a Wnt-independent mechanism regulates cardiomyocyte growth. Proc. Natl. Acad. Sci. U. S. A. **100:**4610–4615.
19. **Hecht, A., C. M. Litterst, O. Huber, and R. Kemler.** 1999. Functional characterization of multiple transactivating elements in beta-catenin, some of which interact with the TATA-binding protein in vitro. J. Biol. Chem. **274:** 18017–18025.

20. **Honsho, S., et al.** 2009. Pressure-mediated hypertrophy and mechanical stretch induces IL-1 release and subsequent IGF-1 generation to maintain compensative hypertrophy by affecting Akt and JNK pathways. Circ. Res. **105:**1149–1158.
21. **Kaplan, S. R., et al.** 2004. Structural and molecular pathology of the heart in Carvajal syndrome. Cardiovasc. Pathol. **13:**26–32.
22. **Kaplan, S. R., et al.** 2004. Remodeling of myocyte gap junctions in arrhythmogenic right ventricular cardiomyopathy due to a deletion in plakoglobin (Naxos disease). Heart Rhythm **1:**3–11.
23. **Kirchhof, P., et al.** 2006. Age- and training-dependent development of arrhythmogenic right ventricular cardiomyopathy in heterozygous plakoglobin-deficient mice. Circulation **114:**1799–1806.
24. **Kostetskii, I., et al.** 2005. Induced deletion of the N-cadherin gene in the heart leads to dissolution of the intercalated disc structure. Circ. Res. **96:** 346–354.
25. **Li, J., et al.** 2008. N-cadherin haploinsufficiency affects cardiac gap junctions and arrhythmic susceptibility. J. Mol. Cell. Cardiol. **44:**597–606.
26. **Li, J., et al.** 2005. Cardiac-specific loss of N-cadherin leads to alteration in connexins with conduction slowing and arrhythmogenesis. Circ. Res. **97:**474–481.
27. **Lombardi, R., et al.** 2009. Genetic fate mapping identifies second heart field progenitor cells as a source of adipocytes in arrhythmogenic right ventricular cardiomyopathy. Circ. Res. **104:**1076–1084.
28. **Maeda, O., et al.** 2004. Plakoglobin (gamma-catenin) has TCF/LEF family-dependent transcriptional activity in beta-catenin-deficient cell line. Oncogene **23:**964–972.
29. **Maher, M. T., A. S. Flozak, A. M. Stocker, A. Chenn, and C. J. Gottardi.** 2009. Activity of the beta-catenin phosphodestruction complex at cell-cell contacts is enhanced by cadherin-based adhesion. J. Cell Biol. **186:**219–228.
30. **Marcus, F. I., et al.** 2010. Diagnosis of arrhythmogenic right ventricular cardiomyopathy/dysplasia: proposed modification of the task force criteria. Circulation **121:**1533–1541.
31. **McKoy, G., et al.** 2000. Identification of a deletion in plakoglobin in arrhythmogenic right ventricular cardiomyopathy with palmoplantar keratoderma and woolly hair (Naxos disease). Lancet **355:**2119–2124.
32. **Meier, H., et al.** 2009. Crucial role of interleukin-6 in the development of norepinephrine-induced left ventricular remodeling in mice. Cell. Physiol. Biochem. **23:**327–334.
33. **Miravet, S., et al.** 2002. The transcriptional factor Tcf-4 contains different binding sites for beta-catenin and plakoglobin. J. Biol. Chem. **277:**1884–1891.
34. **O'Gorman, S., N. A. Dagenais, M. Qian, and Y. Marchuk.** 1997. Protamine-Cre recombinase transgenes efficiently recombine target sequences in the male germ line of mice, but not in embryonic stem cells. Proc. Natl. Acad. Sci. U. S. A. **94:**14602–14607.
35. **Pan, J., et al.** 1998. Involvement of gp130-mediated signaling in pressure overload-induced activation of the JAK/STAT pathway in rodent heart. Heart Vessels **13:**199–208.
36. **Pilichou, K., et al.** 2009. Myocyte necrosis underlies progressive myocardial dystrophy in mouse dsg2-related arrhythmogenic right ventricular cardiomyopathy. J. Exp. Med. **206:**1787–1802.
37. **Protonotarios, N., et al.** 1986. Cardiac abnormalities in familial palmoplantar keratosis. Br. Heart J. **56:**321–326.
38. **Qu, J., et al.** 2007. Cardiac-specific haploinsufficiency of beta-catenin attenuates cardiac hypertrophy but enhances fetal gene expression in response to aortic constriction. J. Mol. Cell. Cardiol. **43:**319–326.
39. **Rodríguez, C. I., et al.** 2000. High-efficiency deleter mice show that FLPe is an alternative to Cre-loxP. Nat. Genet. **25:**139–140.
40. **Ruiz, P., et al.** 1996. Targeted mutation of plakoglobin in mice reveals essential functions of desmosomes in the embryonic heart. J. Cell Biol. **135:**215–225.
41. **Saffitz, J. E.** 2009. Arrhythmogenic cardiomyopathy and abnormalities of cell-to-cell coupling. Heart Rhythm **6**(8 Suppl,)**:**S62–S65.
42. **Sen-Chowdhry, S., R. D. Morgan, J. C. Chambers, and W. J. McKenna.** 2010. Arrhythmogenic cardiomyopathy: etiology, diagnosis, and treatment. Annu. Rev. Med. **61:**233–253.
43. **Sheikh, F., et al.** 2006. Alpha-E-catenin inactivation disrupts the cardiomyocyte adherens junction, resulting in cardiomyopathy and susceptibility to wall rupture. Circulation **114:**1046–1055.
44. **Sohal, D. S., et al.** 2001. Temporally regulated and tissue-specific gene manipulations in the adult and embryonic heart using a tamoxifen-inducible Cre protein. Circ. Res. **89:**20–25.
45. **Staal, F. J., M. Noort Mv, G. J. Strous, and H. C. Clevers.** 2002. Wnt signals are transmitted through N-terminally dephosphorylated beta-catenin. EMBO Rep. **3:**63–68.
46. **Thiene, G., D. Corrado, and C. Basso.** 2007. Arrhythmogenic right ventricular cardiomyopathy/dysplasia. Orphanet J. Rare Dis. **2:**45.
47. **Williamson, L., et al.** 2006. Pemphigus vulgaris identifies plakoglobin as key suppressor of c-Myc in the skin. EMBO J. **25:**3298–3309.
48. **Yang, Z., et al.** 2006. Desmosomal dysfunction due to mutations in desmoplakin causes arrhythmogenic right ventricular dysplasia/cardiomyopathy. Circ. Res. **99:**646–655.
49. **Zhou, J., et al.** 2007. Upregulation of gamma-catenin compensates for the loss of beta-catenin in adult cardiomyocytes. Am. J. Physiol. Heart Circ. Physiol. **292:**H270–H276.
50. **Zhurinsky, J., M. Shtutman, and A. Ben-Ze'ev.** 2000. Differential mechanisms of LEF/TCF family-dependent transcriptional activation by beta-catenin and plakoglobin. Mol. Cell. Biol. **20:**4238–4252.
51. **Zhurinsky, J., M. Shtutman, and A. Ben-Ze'ev.** 2000. Plakoglobin and beta-catenin: protein interactions, regulation and biological roles. J. Cell Sci. **113**(Pt. 18)**:**3127–3139.